Numerical analysis of wave-induced fluid flow effects on seismic data: Application to monitoring of CO_2 storage at the Sleipner field

J. Germán Rubino,[1,2] Danilo R. Velis,[3] and Mauricio D. Sacchi[4]

Received 15 September 2010; revised 12 November 2010; accepted 21 December 2010; published 18 March 2011.

[1] In this work we analyze how patchy distributions of CO_2 and brine within sand reservoirs may lead to significant attenuation and velocity dispersion effects, which in turn may have a profound impact on surface seismic data. The ultimate goal of this paper is to contribute to the understanding of these processes within the framework of the seismic monitoring of CO_2 sequestration, a key strategy to mitigate global warming. We first carry out a Monte Carlo analysis to study the statistical behavior of attenuation and velocity dispersion of compressional waves traveling through rocks with properties similar to those at the Utsira Sand, Sleipner field, containing quasi-fractal patchy distributions of CO_2 and brine. These results show that the mean patch size and CO_2 saturation play key roles in the observed wave-induced fluid flow effects. The latter can be remarkably important when CO_2 concentrations are low and mean patch sizes are relatively large. To analyze these effects on the corresponding surface seismic data, we perform numerical simulations of wave propagation considering reservoir models and CO_2 accumulation patterns similar to the CO_2 injection site in the Sleipner field. These numerical experiments suggest that wave-induced fluid flow effects may produce changes in the reservoir's seismic response, modifying significantly the main seismic attributes usually employed in the characterization of these environments. Consequently, the determination of the nature of the fluid distributions as well as the proper modeling of the seismic data constitute important aspects that should not be ignored in the seismic monitoring of CO_2 sequestration problems.

Citation: Rubino, J. G., D. R. Velis, and M. D. Sacchi (2011), Numerical analysis of wave-induced fluid flow effects on seismic data: Application to monitoring of CO_2 storage at the Sleipner field, *J. Geophys. Res.*, *116*, B03306, doi:10.1029/2010JB007997.

1. Introduction

[2] Since October 1996, CO_2 has been injected into the Utsira Sand, a major saline aquifer at the Sleipner field, offshore Norway, with more than 11 million tonnes currently in the reservoir [*Chadwick et al.*, 2010]. This operation was the world's first industrial scale CO_2 injection project designed specifically as a greenhouse gas mitigation measure [*Chadwick et al.*, 2005]. Since then, a number of other sequestration sites were selected and CO_2 is currently being injected at various places worldwide, including either depleted hydrocarbon reservoirs or deep saline aquifers, as in the case of the Utsira Sand [*Lumley et al.*, 2010; *Lumley*, 2010].

[3] The Utsira Sand is a weakly consolidated sandstone lying at depths between 800 m and 1100 m around Sleipner. Internally it contains thin intrareservoir shale layers, having typical thicknesses of 1–2 m [*Zweigel et al.*, 2004]. The CO_2 is injected at a supercritical state near the bottom of the Utsira Sand, and it rises due to buoyancy effects until it reaches flow barriers such as the thin shale layers and the top seal shale. Beneath each intrareservoir shale, CO_2 accumulates following the structural relief and forms layers of up to a few meters thick [*Arts et al.*, 2004a, 2008]. Seismic methods enable to identify these thin layers as bright subhorizontal reflections, which are mainly caused by the high compressibility of the CO_2 as compared to that of the brine, and by constructive tuning effects of the top and bottom reflections at the CO_2 accumulations [*Arts et al.*, 2004b].

[4] The presence of CO_2 in the pore space of the rock produces a lowering of the compressional velocity which, in turn, may induce significant pushdown of reflections within or below the CO_2 plume. This effect, which is clearly seen in the time-lapse seismic data of the Sleipner field, can be used to obtain additional information about the reservoir

[1] Institute of Geophysics, University of Lausanne, Lausanne, Switzerland.
[2] Formerly at CONICET, Facultad de Ciencias Astronómicas y Geofísicas, Universidad Nacional de La Plata, La Plata, Argentina.
[3] CONICET, Facultad de Ciencias Astronómicas y Geofísicas, Universidad Nacional de La Plata, La Plata, Argentina.
[4] Department of Physics, University of Alberta, Edmonton, Alberta, Canada.

0148-0227/11/2010JB007997

[*Arts et al.*, 2004b; *Chadwick et al.*, 2005; *Gadheri and Landrø*, 2009].

[5] While the plume reflectivity can be explained by the presence of the CO_2-bearing thin layers, the velocity pushdown observed beneath the CO_2 plume at the Sleipner field is too large for the estimated amount of CO_2 present at such thin layers. This fact led *Chadwick et al.* [2005] to propose a model in which the CO_2 plume is partitioned into (1) a main component of high saturation (about 0.9) trapped in thin layers beneath the intrareservoir mudstones and (2) a lesser component of low saturation in between the layers (diffuse CO_2). In addition, these authors observed that to match both the observed reflectivity and the velocity pushdown, the saturation of the second component varies from nearly 0.1 in the axial parts of the plume, to less than 0.01 in its outer parts, and they estimated that about 13% of the known injected CO_2 corresponds to the diffuse component. On the other hand, the high saturation component is trapped in thin layers of up to 10 meters thick, progressively increasing their lateral extents with time.

[6] In a recent paper, *Rubino and Velis* [2011] observed that wave-induced fluid flow effects, which are also called mesoscopic effects, may be very significant in media similar to the Utsira Sand containing patchy CO_2-brine distributions. This is particularly true for CO_2 saturations near 0.1. This attenuation mechanism is presumably the major cause of seismic attenuation in reservoir rocks at seismic frequencies, and is due to the presence of mesoscopic-scale heterogeneities, i.e., inhomogeneities larger than the pore size but smaller than the predominant wavelengths [*White*, 1975; *White et al.*, 1975; *Pride et al.*, 2004; *Carcione and Picotti*, 2006].

[7] The results found by *Rubino and Velis* [2011], together with the fact that very low CO_2 saturation values are expected to be present in the reservoir (diffuse component) at the Sleipner field, encouraged us to study the role of wave-induced fluid flow effects on the seismic data usually employed in the monitoring of CO_2 sequestration problems. With this objective, in this work we first analyze the statistical behavior of the attenuation and velocity dispersion of compressional waves traveling through rocks containing highly heterogeneous distributions of CO_2 and brine in the pore space, and consider different saturation levels and geometric characteristics for the CO_2 patches. Later, we perform numerical simulations of wave propagation in order to study the role played by the nature of the fluid distributions in the seismic data of these environments.

[8] In our experiments, we assume that the heterogeneous distribution of CO_2 and brine in the pore space is patchy. The issue whether the distribution of these fluids within the Utsira Sand is patchy or homogeneous is an open question, for there is no clear evidence to date. It is also an open question whether a patchy CO_2 saturation produces significant effects in conventional surface seismic data [*Lumley*, 2010]. For these reasons, one of the ultimate goals of this investigation is to bring light to this subject. The results of our analysis using reservoir models similar to that found at the Sleipner field show that the nature of the fluid distributions, i.e., patchy or homogeneous, as well as the patch size play key roles in the main characteristics of the seismic data of these geological formations, especially in the presence of regions containing low CO_2 saturation levels. As a consequence studies based on simplifications, such as those that rely on Gassmann's equations and elastic modeling, may not be appropriate for accurate quantitative analysis involved in seismic monitoring of CO_2 sequestration problems.

2. Mesoscopic Attenuation and Velocity Dispersion of Rocks Containing Patchy CO_2-Brine Distributions

[9] As mentioned in section 1, the propagation of seismic waves in rocks containing mesoscopic-scale heterogeneities in the fluid or frame properties may induce fluid flow. This physical process constitutes the dominant P wave attenuation mechanism in reservoir rocks at seismic frequencies and can be understood as follows: when a compressional wave squeezes a heterogeneous fluid-saturated porous material, the different regions of the medium, due to their distinct elastic properties, may undergo different pore fluid pressures. This, in turn, produces fluid flow and thus generates energy loss and velocity dispersion.

[10] Analyzing mesoscopic effects is a very difficult task. This is due to the fact that, in the low frequency range, the diffusion process associated with the fluid pressure equilibration is a critical issue since the corresponding diffusion lengths are very small as compared with the seismic wavelengths. In this work we employ the numerical upscaling procedure presented by *Rubino et al.* [2009] to study these effects in CO_2-bearing formations. These authors proposed a very efficient strategy to obtain equivalent complex frequency-dependent plane wave moduli for heterogeneous fluid-saturated porous rocks. In their method, a representative fluid-saturated rock sample containing mesoscopic-scale heterogeneities is subjected to an oscillatory compressibility test. Then, the equivalent undrained complex plane wave modulus $\overline{M}_c(\omega)$ is expressed in terms of the time-harmonic compression and the complex oscillatory volume change, which is estimated solving Biot's equations of motion in the space-frequency domain under the corresponding boundary conditions. This complex frequency-dependent modulus permits to analyze the behavior of attenuation and phase velocity as functions of frequency in heterogeneous fluid-saturated porous media. For the sake of completeness, we include the main equations of the numerical upscaling procedure in the Appendix A.

[11] With the aim of analyzing the amount of attenuation and velocity dispersion caused by heterogeneous fluid distributions in CO_2-bearing environments, let us consider the Utsira Sand with a spatially variable CO_2-brine distribution in the form of irregular patches fully saturated with CO_2 and zones fully saturated with brine. We take into account neither mixing nor capillary forces, and assume that the two fluids occupy different mesoscopic regions of the model. Also, we neither consider chemical interaction between pore fluids and rock frame nor solubility effects. We generate these binary heterogeneous fluid distributions using stochastic fractal fields based on the so-called von Karman self-similar correlation functions, as explained by *Rubino and Velis* [2011], and consider different correlation lengths and CO_2 saturations. Figure 1 shows some examples of the rock samples containing quasi-fractal fluid distributions considered in this work.

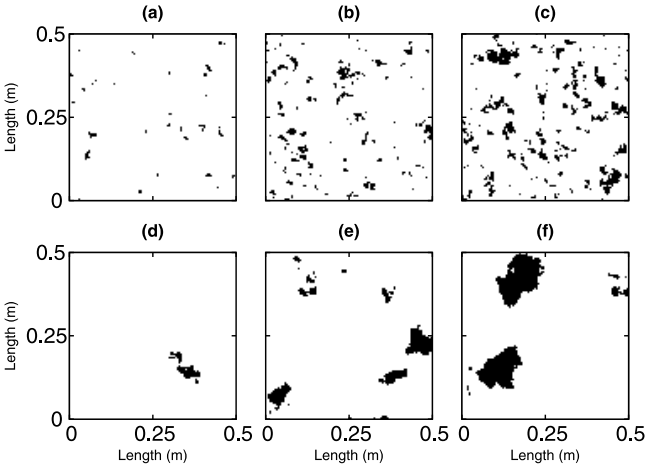

Figure 1. Samples of quasi-fractal distributions of CO_2 and brine in the Utsira Sand for two correlation lengths, (a, b, and c) $a = 0.01$ m and (d, e, and f) $a = 0.1$ m, and three different CO_2 saturations, $S_{CO_2} = 0.01$, 0.05, and 0.1, from left to right.

[12] In order to compute the wave-induced fluid flow effects, we require the rock frame and pore fluids physical parameters. In this sense, we assume that the solid matrix of the rock sample is homogeneous and corresponds to the Utsira Sand, with properties given by *Arts et al.* [2004b]. Following this work, we take a rock porosity $\phi = 0.37$, mineral bulk modulus $K_s = 36.9$ GPa and solid grains density $\rho_s = 2.65$ gr/cm^3. Also, we consider a brine density $\rho_w = 1.09$ gr/cm^3 and bulk modulus $K_w = 2.3$ GPa. In addition we set, for full water saturation, $V_P = 2.05$ km/s and $V_S = 0.643$ km/s [*Arts et al.*, 2004b]. Thus, using the inverse Gassmann's equation and the relation between shear velocity, bulk density and shear modulus, we obtain the rock frame bulk modulus $K_m = 2.68$ GPa, and the shear modulus $\mu_m = 0.857$ GPa. Also, water viscosity is taken to be $\eta_w = 1$ cP and rock permeability $\kappa = 1$ D.

[13] We calculate the CO_2 density and bulk modulus employing the equation of state proposed by *Duan et al.* [1992], considering a temperature $T = 37$°C and pressure $P = 10$ MPa, which are representative values for the reservoir under consideration. Thus, in the numerical experiments we set $\rho_{CO_2} = 0.693$ gr/cm^3 and $K_{CO_2} = 0.0229$ GPa. In addition, we use the Sutherland's formulae to compute CO_2 viscosity as a function of temperature, obtaining $\eta_{CO_2} = 1.56 \times 10^{-4}$ P.

[14] Since we are dealing with rocks having local properties drawn from a certain probability distribution, we apply a Monte Carlo analysis similar to that suggested by *Rubino et al.* [2009] to extract the statistical characteristics of the equivalent compressional phase velocity and quality factor. For this purpose we consider different overall saturation values, frequencies and correlation lengths, and for each set of parameters we generate a large number of realizations, N_E. Next, for each one of them we obtain the equivalent compressional phase velocity and quality factor and calculate their means and standard deviations, which represent the statistical behavior of the samples under consideration. To ensure convergence of the Monte Carlo approach, we consider a criterion similar to that employed by *Rubino et al.* [2009], i.e., for each set of parameters we check that the variances of the equivalent compressional phase velocity and quality factor, as functions of the number of realization, stabilize at constant values after N_E realizations. In practice, in the following experiments this was achieved after about 60 realizations.

[15] Figure 2 shows, as function of frequency, the statistical behavior of the equivalent compressional phase velocity for correlation lengths $a = 0.01$ m and $a = 0.1$ m. In both cases, we consider three typical "low" CO_2 saturation values (0.01, 0.05 and 0.1) which are expected to be found in the area containing the diffuse component of this fluid within the Utsira Sand. We can observe that velocity dispersion is negligible for very small CO_2 patch sizes (Figure 2a); however, when the correlation length is larger the velocity dispersion effects are more significant (Figure 2b). In fact, we can observe that for a correlation length $a = 0.1$ m, the mean

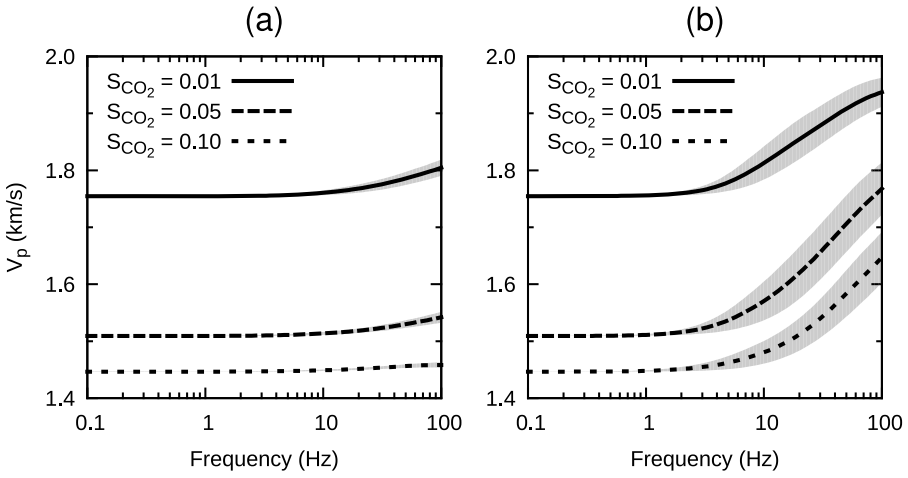

Figure 2. Mean equivalent compressional phase velocity as a function of frequency for three "low" CO_2 saturations and two correlation lengths: (a) 0.01 m and (b) 0.10 m. Shaded gray areas indicate their corresponding standard deviation intervals.

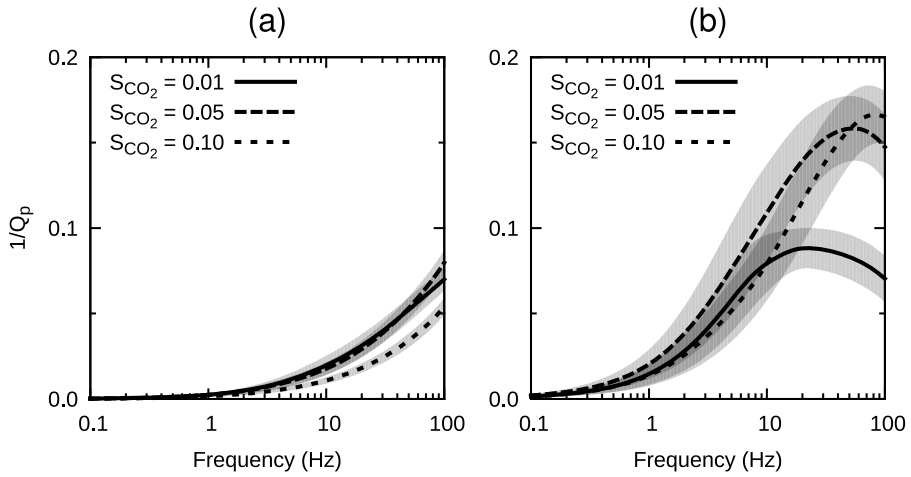

Figure 3. Mean equivalent inverse quality factor as a function of frequency for three "low" CO_2 saturations and two correlation lengths: (a) 0.01 m and (b) 0.1 m. Shaded gray areas indicate their corresponding standard deviation intervals.

equivalent compressional velocity may increase significantly with frequency, showing in some cases a relative increment above 15% in the frequency range considered. Figure 2b shows that wave-induced fluid flow effects may play a key role in the seismic monitoring of CO_2 sequestration processes. The velocity dispersion effects shown in this plot may affect strongly the velocity pushdown as well as the reflectivity of the seismic data, which in turn may lead to an incorrect interpretation of the injection progress within these environments. On the contrary, a deeper understanding of these effects may help to improve the characterization of these media, since the additional information provided by the observed dependency between velocity and frequency could be used.

[16] Similarly, Figure 3 illustrates, as function of frequency, the statistical behavior of the equivalent inverse quality factor for the same correlation lengths and CO_2 saturations. We observe that in both sets of experiments very significant loss levels can take place, with Q values lower than 10 in some cases. It is interesting to remark that, as expected, the attenuation levels obtained for a correlation length a = 0.1 m are much more significant than those obtained for a = 0.01 m. In addition, for the experiments with a = 0.1 m, the loss is less important for S_{CO_2} = 0.01 than for the other two considered CO_2 concentrations (see Figure 3b). Nevertheless, in all cases the mean quality factor takes values below 20 for frequencies above 5 Hz, approximately.

[17] Observing Figures 2 and 3, it turns out to be very interesting to notice the lack of uncertainty at low frequencies, which is expected since for relatively large wavelengths the medium is *seen* by the seismic wave as homogeneous, independently of the realization. As frequency increases, the seismic wave starts to be affected by the differences among realizations, with the consequent increase in the variances observed in the plots.

[18] We carry out a similar analysis for CO_2 saturations in the range 0.15–0.9. With this aim, we extract the statistical behaviors of the equivalent compressional phase velocity and inverse quality factor of different sets of rock samples involving correlation lengths a = 0.01 m and a = 0.1 m, and four "high" CO_2 saturations, S_{CO_2} = 0.15, 0.2, 0.5, and 0.9. It is important to state here that mesoscopic attenuation and velocity dispersion turned out to be negligible in the case S_{CO_2} = 0.9, and thus, the corresponding curves were not included in the plots for clarity.

[19] In the case of the smallest patch size, we found that the velocity dispersion effects in the frequency range considered in this work, as well as the standard deviations, are negligible (see Figure 4a). However, for a larger correlation length (a = 0.1 m) the velocity dispersion effects become more significant, mainly for CO_2 saturation values below 0.2 and frequencies above 10 Hz (see Figure 4b).

[20] Figure 5 shows, as function of frequency, the statistical behavior of the equivalent inverse quality factor for the same correlation lengths and CO_2 saturations. We observe that even at these relatively high CO_2 concentrations the mesoscopic loss may be very significant, specially for the largest correlation length. In addition, the mesoscopic effects are smaller for the highest CO_2 saturations shown in Figure 5.

[21] From this analysis we can conclude that wave-induced fluid flow effects at seismic frequencies may be very significant in CO_2-bearing environments similar to the Utsira Sand. We also observed that these effects are particularly enhanced for low CO_2 saturations (S_{CO_2} = 0.2 and below) and relatively large (a = 0.1) patch sizes. On the contrary, mesoscopic effects are negligible for very high CO_2 saturation values. In the frame of seismic monitoring of CO_2 sequestration processes as that currently taking place at the Sleipner field, these results suggest that wave-induced fluid flow effects may play a key role at those parts of the plume where CO_2 is present at very low concentrations, such as the diffuse component at the Utsira Sand. In contrast, these effects are expected to be negligible at those parts of the plume where CO_2 accumulates with very high saturation values, as in the case of the CO_2-bearing thin layers within the same reservoir. Consequently, we believe that this loss mechanism should not be neglected when analyzing time lapse seismic data, for their effects may be

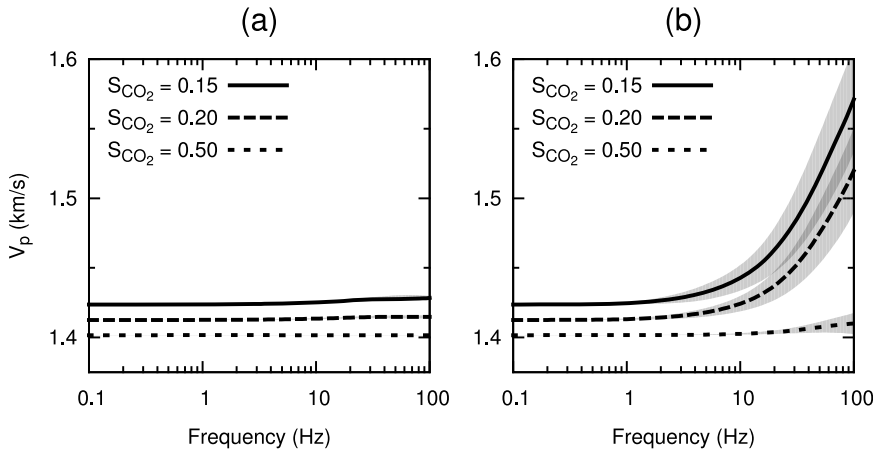

Figure 4. Mean equivalent compressional phase velocity as a function of frequency for three "high" CO_2 saturations and two correlation lengths: (a) 0.01 m and (b) 0.10 m. Shaded gray areas indicate their corresponding standard deviation intervals.

very significant in the observed reflectivity and pushdown, as we will show in section 3.

3. Wave-Induced Fluid Flow Effects on Seismic Data

[22] Different authors performed seismic modeling to interpret real data from the Sleipner field. For instance, *Arts et al.* [2004b] employed convolutional seismic modeling to analyze reflection amplitude-CO_2 thickness relationships in the Utsira Sand. *Arts et al.* [2007] performed numerical simulations of elastic wave propagation in 2D domains considering models containing low velocity zones related to patchy CO_2 distributions located between thin layers containing very high concentrations of CO_2. These papers, as most works dealing with seismic wave propagation in the Sleipner field, did not consider potential attenuation and velocity dispersion effects associated with heterogeneous fluid distributions. In this sense, in our opinion the role of mesoscopic effects in seismic monitoring of CO_2 sequestration has not received as much attention as it deserves. In fact, as far as we know, there are no articles that study this topic in detail, with the exception of the paper by *Carcione et al.* [2006]. These authors quantified these effects at the Utsira Sand, and observed that mesoscopic loss may be very significant at this geological formation. However, to obtain this information they employed the analytical White's model [*White*, 1975], which is strictly valid for spherical gas patches, and did not analyze in depth the role of this physical mechanism in the seismic data.

[23] The numerical experiments performed in section 2 let us observe that wave-induced fluid flow effects may be very significant at CO_2-bearing formations similar to that found at the Sleipner field, and thus, this physical mechanism may affect significantly the main seismic attributes usually employed to characterize these environment. With this motivation, in this section we perform numerical simulations of wave propagation taking into account mesoscopic attenu-

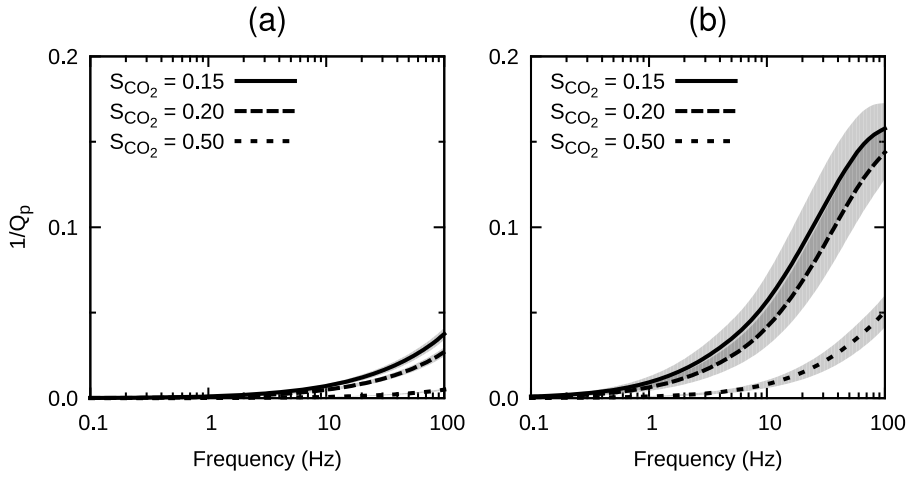

Figure 5. Mean equivalent inverse quality factor as a function of frequency for three "high" CO_2 saturations and two correlation lengths: (a) 0.01 m and (b) 0.1 m. Shaded gray areas indicate their corresponding standard deviation intervals.

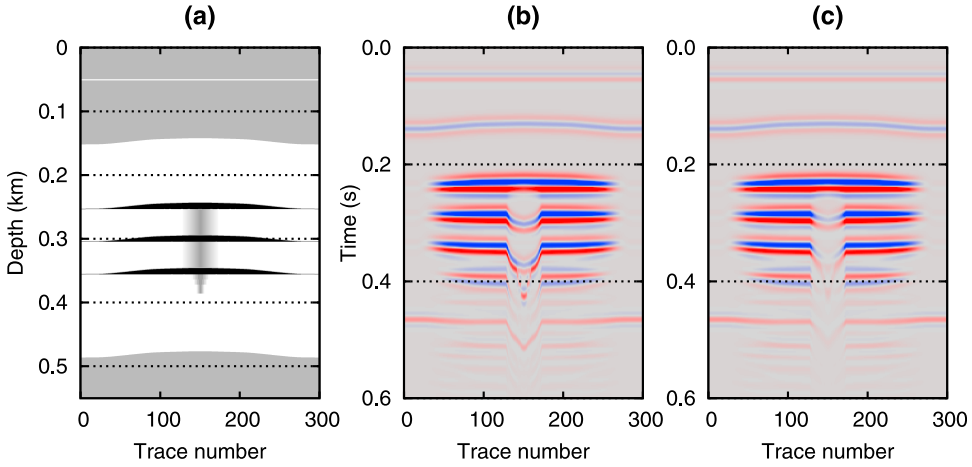

Figure 6. (a) Scheme of a very simple geological model used to analyze the mesoscopic effects on the seismic data of formations containing CO_2. The black thin areas indicate the main component of CO_2, while the narrow gray shaded areas indicate the presence of the diffuse component of CO_2, with saturations varying from 0.1 in their axial parts to zero in their outer parts. (b and c) Seismic responses of the simple model shown in Figure 6a considering the mesoscopic effects of the CO_2-bearing regions for two correlation lengths: 0.01 m and 0.1 m.

ation and velocity dispersion effects due to the presence of highly heterogeneous distributions of CO_2 and brine.

[24] Performing numerical simulations of seismic wave propagation in porous media containing mesoscopic-scale heterogeneities is computationally very expensive or not even feasible. As mentioned before, this is mainly due to the fact that, in the low frequency range, the diffusion lengths associated with the fluid pressure equilibration processes taking place at the mesoscopic heterogeneities are very small as compared with the predominant seismic wavelengths. To overcome these difficulties, in this section we use the upscaling procedure briefly explained before to replace each one of the highly heterogeneous porous regions composing the geological model by equivalent viscoelastic solids, and solve the viscoelastic equation in the space-frequency domain. These equivalent viscoelastic solids have the same bulk density, attenuation and velocity dispersion as the original fluid-saturated porous samples and thus, they include the mesoscopic effects that are expected to arise in these environments. This approach is very convenient, since employing the viscoelastic equation is computationally much less expensive than any numerical procedure based on the discretization of the full Biot's equations for the same order of accuracy.

[25] Though usually real reservoirs are very complex, employing simplified geometries may help to extract the essence of the physical processes taking place in the media. In this sense, in this section we analyze zero-offset (normal incidence) seismic sections by considering one-dimensional numerical simulations of wave propagation through two-dimensional geological models that represent different CO_2 injection scenarios, including different patch sizes, saturation values and CO_2 distributions. The details of the utilized modeling procedure are provided in Appendix B.

3.1. A Very Simple Model

[26] As a first approach to analyze the wave-induced fluid flow effects on seismic data of formations containing CO_2, let us consider a very simple geological model which shares some characteristics with the Sleipner field. The model is depicted in Figure 6a, where we observe that the CO_2 plume is located within a 333 m thick sand reservoir, with similar physical properties as compared with the Utsira Sand previously detailed in this work. The sand (white areas in Figure 6a) is embedded between two homogeneous shale halfspaces (top and bottom gray areas) with properties given by *Arts et al.* [2004b], i.e., V_p = 2.27 km/s, V_s = 0.85 km/s, and ρ = 2.1 gr/cm^3.

[27] Within the reservoir, the CO_2 is symmetrically distributed, and is partitioned into a main component of CO_2 with very high saturation (S_{CO_2} = 0.9), and a lesser component of diffuse CO_2 ($S_{CO_2} \leq 0.1$). The main component of CO_2 is accumulated in three layers with thicknesses ranging from 10 m in the axial part of the model, to almost zero in its outer parts (black thin areas in Figure 6a). These accumulations are located beneath ultrathin shale layers with thicknesses of 1 m. The shallowest ultrathin shale layer is located 100 m below the top of the sand reservoir, and the separation between consecutive shale layers is 50 m. The injection point is located 30 m below the deepest high-saturation CO_2 accumulation, at a depth of about 380 m. The diffuse component of CO_2 is trapped between the high saturation layers around the central part of the plume (gray shaded areas centered at trace number 150 in Figure 6a). This region is 43 traces wide and its CO_2 saturation varies almost linearly from 0.1 in its axial part to zero in its outer part. In all the numerical experiments studied in this work, we consider a 30 Hz-Ricker wavelet.

[28] Figures 6b and 6c show the seismic responses obtained for this very simple model considering the wave-induced fluid flow effects due to the patchy nature of the CO_2-brine distributions for two different correlation lengths, 0.01 m and 0.1 m, respectively. We can see very strong reflections associated with the presence of the thin layers containing very high CO_2 saturations. They are produced by the high contrast between the acoustic impedance of the

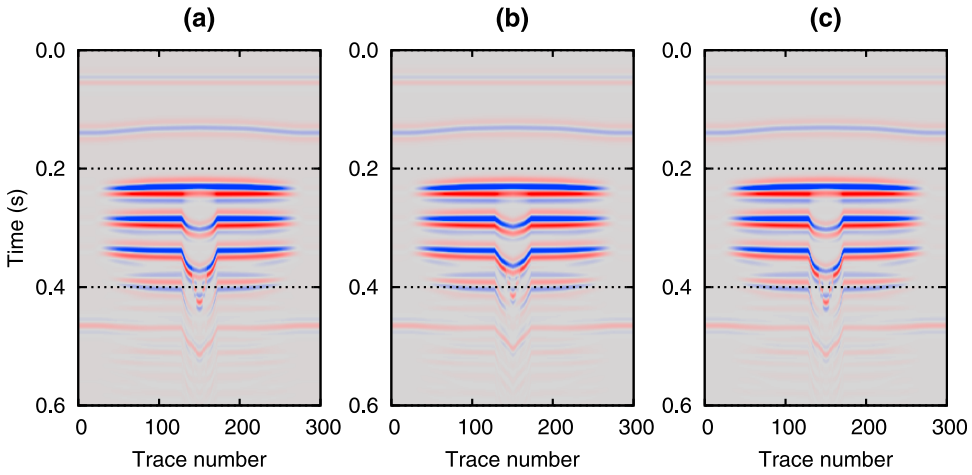

Figure 7. Seismic responses of the simple model shown in Figure 6a after replacing the viscoelastic media by elastic media with the same bulk density and shear velocity, and a mean compressional velocity. Two correlation lengths are considered: (a) 0.01 m and (b) 0.1 m. (c) The same but with a compressional velocity given by Gassmann's formula.

water-saturated sand and those of the thin layers, and by constructive tuning effects of the top and bottom reflections at the CO_2 accumulations. In the case of a Ricker wavelet, such as the source we use to generate the data, the tuning thickness is given by $\sqrt{6}/(2\pi f_0)$, where f_0 is the central frequency [*Chung and Lawton*, 1995]. Since this value is equivalent to a 10 m thick layer for the considered parameters, the reflectivity is more intense in the axial part of the plume, and decreases toward its outer parts where these layers become thinner.

[29] It is also very interesting to notice the velocity pushdown effects on the seismic data, which are more significant, as expected, in the axial part of the plume, too. Besides, we can observe the wave-induced fluid flow effects on the simulated seismic data by noting that the seismic waves experience very strong attenuation effects, mainly in the axial part of the plume and for the largest patch size, as shown in Figure 6c. In fact, in this case, and as a consequence of the very strong mesoscopic loss, it is not possible to recognize easily the reflectivity of the bottom of the sand reservoir in its central part. In addition, by comparing these two sections we can observe the velocity dispersion effects, because the velocity pushdown effects are more significant in the smallest patch size case. These results are in agreement with those found in the previous section, since we observed that mesoscopic attenuation and velocity dispersion effects are very significant in these media, mainly for low CO_2 saturations and the largest patch size considered in this work.

[30] The velocity dispersion effects can be seen more clearly if we reduce the attenuation effects on the seismic data. To do so, we recalculate the seismic response of the model shown in Figure 6a after replacing the viscoelastic media by elastic solids with the same bulk density and shear velocity, but with a compressional velocity given by the frequency average of the equivalent compressional phase velocity in the frequency range where the source energy is concentrated. These data, which are to be compared with those in Figures 6b and 6c, are shown in Figures 7a and 7b. Now, we can observe the velocity pushdown effects on the seismic data more clearly.

[31] Since it is very usual to employ simplifications such as Gassmann's formula and elastic modeling in the seismic monitoring of the injection process of CO_2 [e.g., *Arts et al.*, 2004b], it is very interesting to compare the results considering the mesoscopic effects due to the patchy nature of the fluids distributions in these environments with those obtained employing such simplification. With this objective, Figure 7c shows the results obtained replacing the viscoelastic media by elastic media with the same bulk density and shear velocity, but with a compressional velocity obtained using the Gassmann's formula. Of course, these simulated seismic data include neither attenuation nor velocity dispersion effects. When compared with Figures 6b and 6c, we observe that the greatest discrepancies arise in the largest patch size case. On the other hand, since mesoscopic effects are relatively weak for the smallest patch size, elastic modeling and Gassmann's formula can be used to obtain reasonable estimations of the seismic data in such cases.

[32] To analyze these facts more deeply, Figure 8 shows the traces located in the center of the CO_2 plume extracted from each data set shown in this section. First, let us analyze Figure 8a, which includes the seismic data for the case a = 0.01 m. We observe that the elastic modeling considering a mean velocity and that obtained using Gassmann's formula coincide, as expected, since velocity dispersion effects are negligible for this patch size. Also, comparing these curves with that corresponding to the viscoelastic modeling, we see that reflections are less significant in the latter, which shows the mesoscopic attenuation effects. Thus, these results suggest that in the case of very small patch sizes, although the elastic modeling employing Gassmann's formula can be used to model velocity pushdown effects, the reflectivity amplitudes are found to be overestimated.

[33] The situation depicted in Figure 8b, where a = 0.1 m, is clearly different. In this case, we can see that, because the velocity dispersion effects are no longer negligible, the

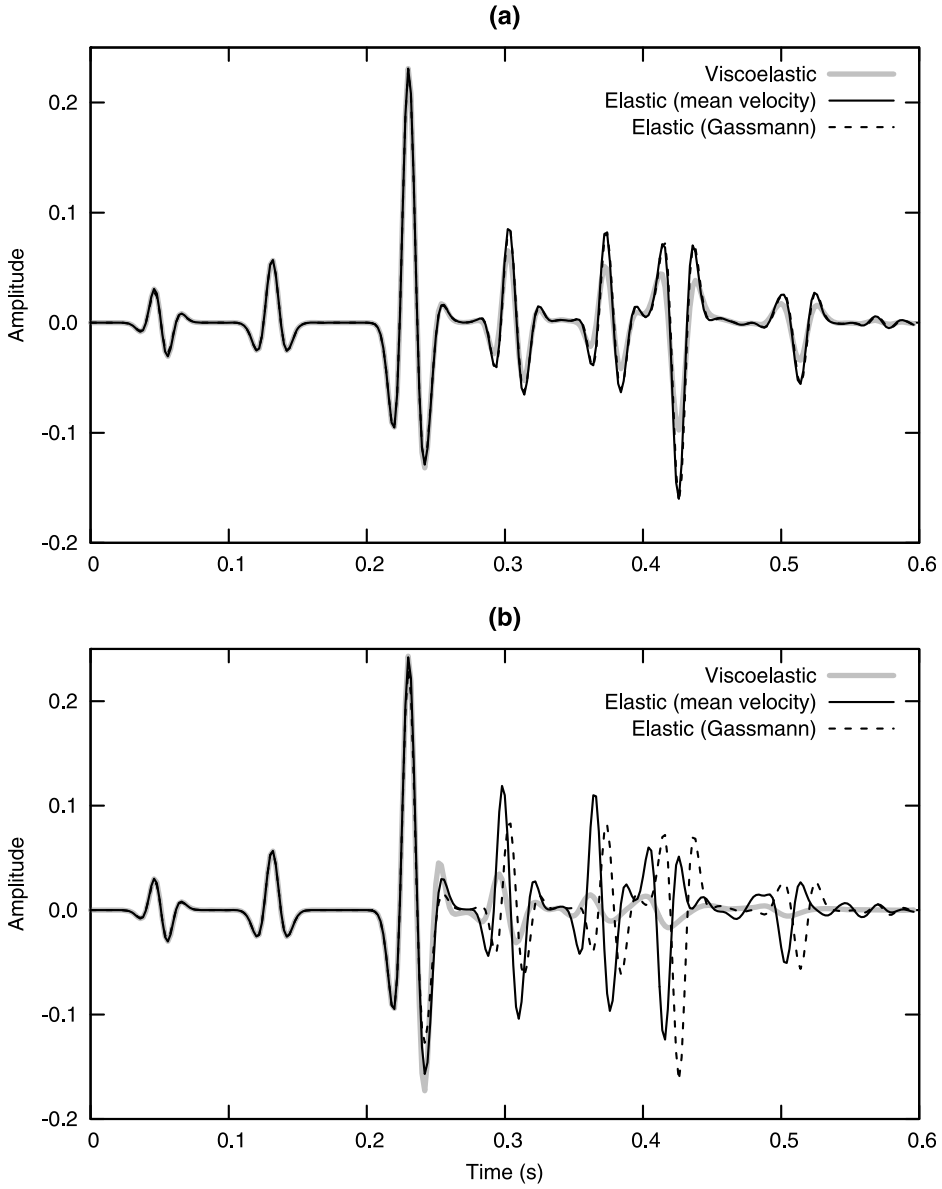

Figure 8. Trace located in the center of the CO_2 plume for the different cases presented before in this section and considering two correlation lengths: (a) 0.01 m and (b) 0.1 m.

elastic modeling considering a mean velocity and that obtained using the Gassmann's formula show significant discrepancies. We observe that these discrepancies are related to differences in reflectivity amplitudes as well as in the arrival time of the different pulses. In addition, comparing these curves with that corresponding to the viscoelastic modeling, we see very significant disagreements between them, because now both attenuation and velocity dispersion effects are very significant. Among the differences, it is interesting to notice the broadening of the different pulses in the viscoelastic modeling as compared with those obtained in the elastic modelings. It turns out to be very clear from these experiments that not taking into account the wave-induced fluid flow effects in the presence of heterogeneous fluid distributions with correlation lengths of about 0.1 m may lead to incorrect interpretations of the seismic data. This is due to the fact that velocity pushdown effects and reflectivity amplitudes, which constitute the main attributes used in seismic characterization of these environments, are highly affected by mesoscopic attenuation and velocity dispersion effects.

[34] The errors in the interpretation of the velocity pushdown (time shift) that might take place when assuming homogeneous fluid distributions instead of patchy distributions might be very significant. This is particularly true for large correlation lengths and thick layers of diffuse CO_2. To quantify these errors, and for the sake of simplicity, we assume that the pushdown associated with any given reflector of the viscoelastic model is approximately equal to that obtained considering an elastic model where the viscoelastic media were replaced by equivalent elastic solids with mean compressional velocities, as explained before in this section. Also, we assume that, for the case of a correlation length of 0.01 m, the pushdown associated with any

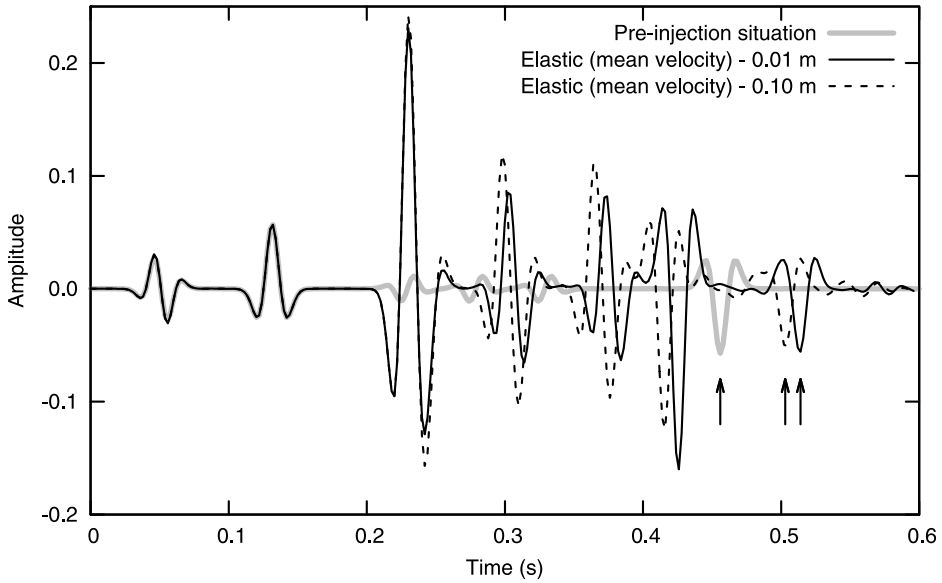

Figure 9. Trace located in the center of the reservoir, before and after the injection, for two different correlation lengths. In the second case, the viscoelastic media were replaced by elastic solids with a compressional velocity given by the frequency average of the equivalent compressional phase velocity. Small arrows indicate the bottom reflector.

given reflector of the viscoelastic model is approximately equal to that of the elastic model with a compressional velocity obtained using Gassmann's formula, as expected from Figure 8a. The seismic responses associated with these models were already shown in Figure 7. The central traces are depicted in Figure 9, together with the trace for the preinjection situation. The reflectors of the bottom of the sand reservoir, in the different cases, are indicated in the plot by small arrows, and have arrival times of about 514, 503 and 456 ms, respectively. Thus, if the distribution of the fluids is patchy with a correlation length of 0.1 m, the pushdown is about 47 ms. On the other hand, if the distribution is homogeneous and Gassmann's modeling is utilized, the pushdown is about 58 ms. This value corresponds to a relative difference of about 23%, showing the importance of velocity dispersion effects due to wave-induced fluid flow when quantifying CO_2 volumes from velocity pushdown information.

[35] We now propose a simple "back-of-the-envelope" analysis to obtain a general expression to estimate the pushdown relative difference that is expected for an arbitrary reservoir column composed of different layers with

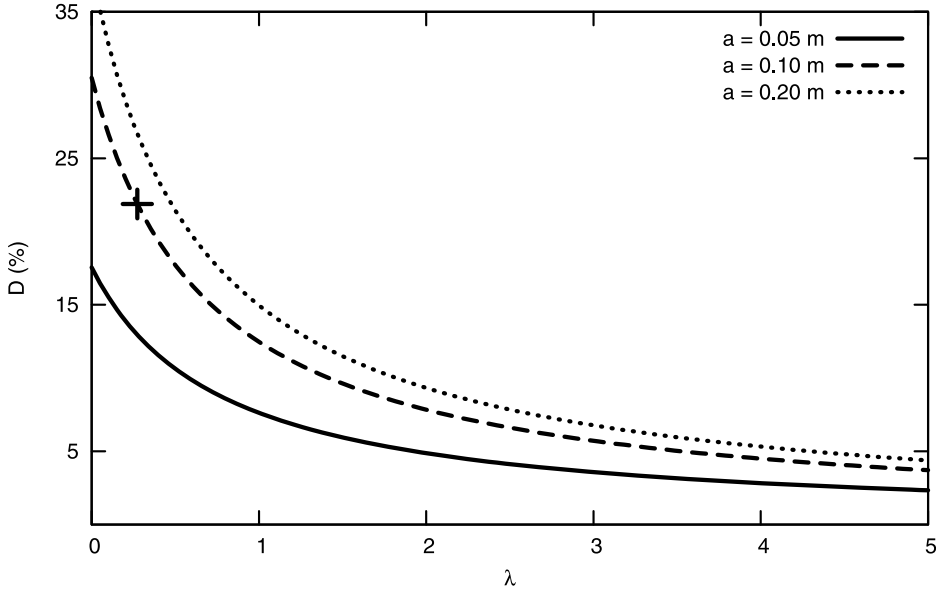

Figure 10. Pushdown relative difference as a function of λ, the ratio between the total thicknesses of the zones containing CO_2 with 90% and 10% saturation, respectively. Values are estimated for three different correlation lengths. The small cross indicates the relative difference in the case depicted in Figure 9.

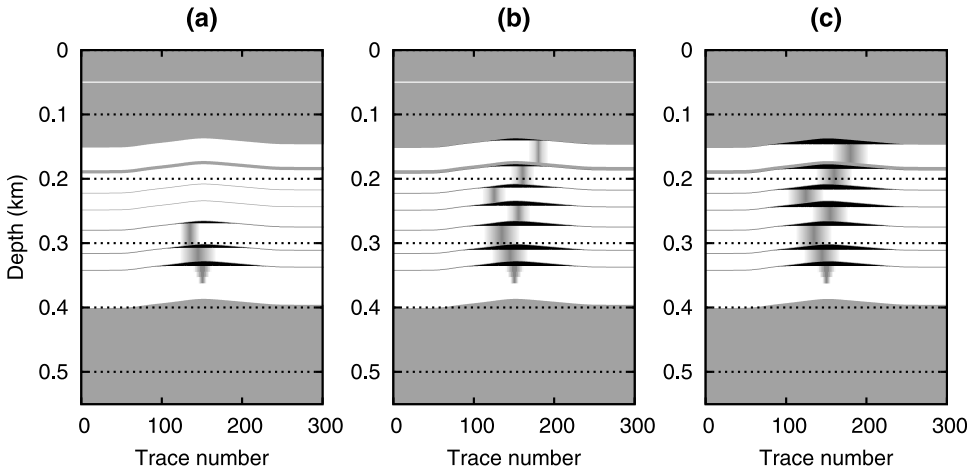

Figure 11. Scheme of the complex geological model used to analyze the mesoscopic effects on seismic data of formations containing CO_2. The black thin areas indicate the main component of CO_2, while the narrow gray shaded areas indicate the presence of the diffuse component of CO_2, with saturations varying from 0.1 in their axial parts to zero in their outer parts. (a–c) Three different injection stages.

either one of two typical CO_2 concentrations, 10% and 90%, as in the case of the axial part of the simple model under study. In the case of normal incidence, the pushdown can be estimated by

$$\Delta t \simeq 2\left(\frac{h_{10}}{V_{10}} + \frac{h_{90}}{V_{90}} - \frac{h_{10}+h_{90}}{V_0}\right), \tag{1}$$

where h_{10} and h_{90} are the total thicknesses of the layers with $S_{CO_2} = 0.1$ and 0.9, respectively, and V_0, V_{10} and V_{90} are the compressional velocities of the reservoir with $S_{CO_2} = 0$, 0.1 and 0.9, respectively. Note that here, V_{10} and V_{90} are the velocities obtained after frequency averaging the equivalent compressional phase velocities in the case of patchy fluid distributions, while they are the velocities obtained using Gassmann's expression in the case of homogeneous fluid distributions. Then, if Δt is the pushdown associated with the homogeneous model and $\Delta t'$ is that associated with the patchy model, and taking into account that the velocity dispersion effects are negligible in the case $S_{CO_2} = 0.9$, it is straightforward to show that the relative difference can be approximated by

$$D = \frac{\Delta t - \Delta t'}{\Delta t'} \simeq \frac{\frac{1}{V_{10}} - \frac{1}{V'_{10}}}{\lambda\left(\frac{1}{V_{90}} - \frac{1}{V_0}\right) + \frac{1}{V'_{10}} - \frac{1}{V_0}}, \tag{2}$$

where $\lambda = h_{90}/h_{10}$, V_{10} is the average velocity of the homogeneous model and V'_{10} is the average velocity of the patchy model. In the particular case of the Utsira Sand, $V_0 = 2.05$ km/s, $V_{10} = 1.454$ km/s, and $V_{90} = 1.41$ km/s. Figure 10 shows D versus λ for three different values of V'_{10}, namely 1.52, 1.56 and 1.58 km/s, which correspond to three different correlation lengths, 0.05, 0.1 and 0.2 m, respectively. It can be observed that, as expected, the thinner the layers with $S_{CO_2} = 0.9$ as compared with the layers with $S_{CO_2} = 0.1$ (i.e., $\lambda \ll 1$), the higher the relative difference. This is expected since wave-induced fluid flow effects, and in particular velocity dispersion effects, are much more significant for $S_{CO_2} = 0.1$ than for $S_{CO_2} = 0.9$. Further, the relative difference increases with correlation length, which is also expected because the dispersion effects are more significant when the patch size is relatively large, as shown in Figures 2 and 4. On the contrary, D is relatively small when little or no diffuse CO_2 is present in the reservoir column ($\lambda \gg 1$). But even in the case that the thickness of the column with diffuse CO_2 is equal to the thickness of the column with $S_{CO_2} = 0.9$ (i.e., $\lambda = 1$), the relative difference is very significant, especially when the patch size is relatively large. In the particular case shown in Figure 9, $h_{90} \simeq 30$ m and $h_{10} \simeq 110$ m. Then $\lambda \simeq 0.27$ and $D \simeq 23$ % (small cross in Figure 10), in agreement with the relative difference determined from the arrival times. In environments such as the Sleipner field (Utsira Sand), $\lambda < 1$, so significant errors might be expected in the interpretation of velocity pushdown if patchy fluid mixing at suitable scales (relatively large patch sizes) is present and simplifications such as Gassmann's formula are employed.

3.2. A Complex Model: Sleipner Field

[36] In order to analyze wave-induced fluid flow effects in a more realistic case, let us consider a complex model to simulate a situation similar to that taking place at the Sleipner field. It is important to state here that the objective of this section is not to reproduce the seismic data from the Sleipner field, but to analyze the importance of the mesoscopic effects in the seismic characterization of environments with similar characteristics.

[37] Figure 11 shows a possible conceptual model at three different stages of the injection process taking place at the Sleipner field. This model was constructed following the available literature on this topic [*Arts et al.*, 2004b, 2007, 2008; *Chadwick et al.*, 2005]. The CO_2 plume is located within a ~250 m thick sandstone (white areas in Figure 11) with properties similar to the Utsira Sand, and it is embedded between two shale halfspaces, corresponding to the top and bottom gray areas in the plots. Within the reservoir, the

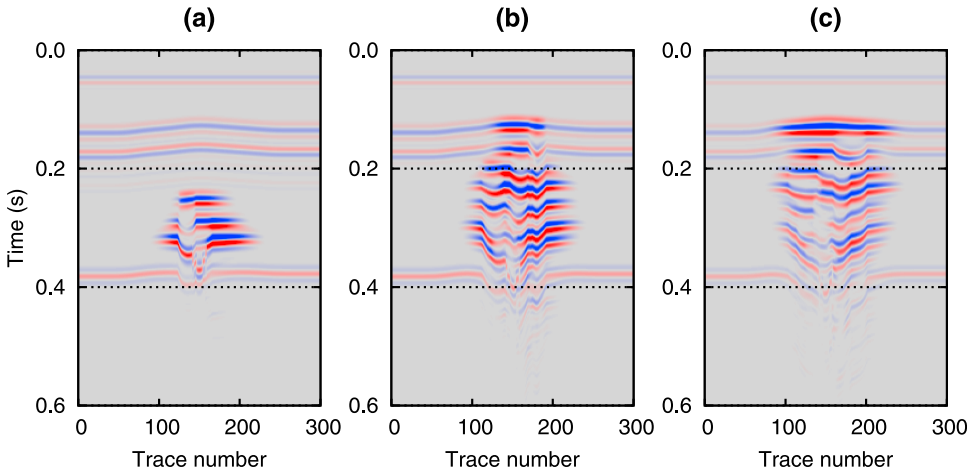

Figure 12. Seismic responses of a model similar to the Sleipner field considering the mesoscopic effects due to the patchy nature of the fluid distributions, for a correlation length of 0.01 m. (a–c) Plots corresponding to the three injection stages depicted in Figure 11.

CO_2 is partitioned into a main component of CO_2 with very high saturation ($S_{CO_2} = 0.9$) and a lesser component of low CO_2 saturation ($S_{CO_2} \leq 0.1$).

[38] The main component of CO_2 accumulates, in the final stage of the injection process, in seven layers with thicknesses ranging from 8 to 10 m in the axial part of the model to almost zero in its outer parts, and are indicated as black thin areas in Figure 11. These accumulations, which increase in number and become wider and thicker as the injection process evolves, are located beneath ultrathin shale layers, with the exception of the uppermost accumulation, which lays beneath the main reservoir cap rock of our conceptual model, i.e., below the top shale halfspace. The ultrathin shale layers have thicknesses of 1 m, except the uppermost shale layer, which has a thickness of 5 m, as it is the case in the Utsira Sand. In addition, the diffuse component of CO_2 that conforms the plume accumulates in regions which are approximately 10 to 43 traces wide with concentrations varying from 0.1 in their axial parts to zero in their outer parts. These accumulations, which are indicated as gray shaded areas in Figure 11, also increase in number and become wider as the injection process evolves. The injection point is located at ~220 m below the top of the reservoir.

[39] The injection of CO_2 in the reservoir produces a dramatic change in its seismic response, as can be seen in Figures 12 and 13, where we show the simulated data considering the wave-induced fluid flow effects due to the patchy nature of the CO_2-brine distributions, for correlation lengths of 0.01 m and 0.1 m, respectively. As in the previous case, we can see very strong reflections associated with the presence of the thin layers containing very high CO_2 saturation. The strongest amplitudes take place mainly at the uppermost accumulation, as well as in the regions where the diffuse CO_2 is not present. The latter is due to significant mesoscopic attenuation effects produced by the

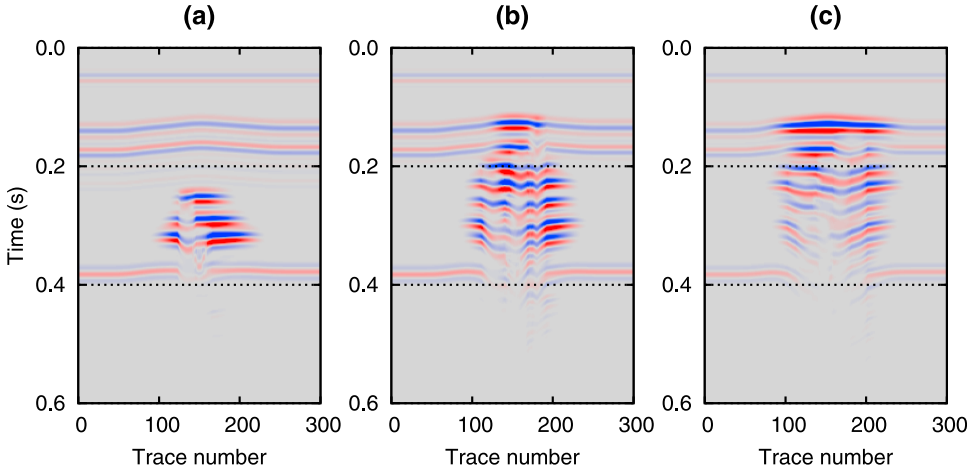

Figure 13. Seismic responses of a model similar to the Sleipner field considering the mesoscopic effects due to the patchy nature of the fluid distributions, for a correlation length of 0.1 m. (a–c) Plots corresponding to the three injection stages depicted in Figure 11.

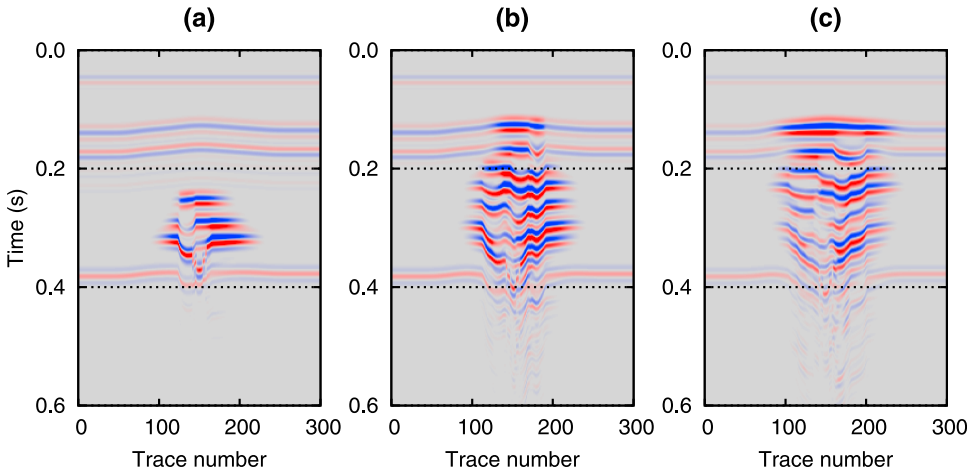

Figure 14. Seismic responses of a model similar to the Sleipner field, obtained replacing the viscoelastic media by elastic media with the same bulk density and shear velocity, but with a compressional velocity given by Gassmann's formula. (a–c) Plots corresponding to the three injection stages depicted in Figure 11.

presence of diffuse CO_2, as well as to reductions of the impedance contrasts between the thin CO_2 accumulations and the media lying above and/or below them.

[40] It is also very interesting to notice the velocity pushdown effects on the simulated data, which are more significant in the axial part of the plume, as expected. We can also observe that the seismic waves experience very strong attenuation effects, mainly in the axial part of the plume, where most of the diffuse CO_2 accumulations are located, and for the largest patch sizes considered in this work. Also, comparing Figures 12 and 13 we can notice the velocity dispersion effects, since the velocity pushdown effects are more significant, as expected, in the smallest patch sizes case.

[41] In order to compare the results obtained considering the wave-induced fluid flow effects with those computed using Gassmann's formula, Figure 14 shows the results obtained replacing the viscoelastic media by elastic media with the same bulk density and shear velocity, but with a compressional velocity obtained using the Gassmann's formula. Comparing these results with those shown in Figures 12 and 13, we can observe very significant discrepancies, mainly for the largest patch size case. For a correlation length of 0.01 m, the discrepancies between the responses of the patchy model and the elastic Gassmann-based model are small. However, when considering $a = 0.1$ m the differences observed both in the attenuation and velocity dispersion, and consequently in reflectivity and pushdown effects, are very important.

[42] Since patchy distributions of CO_2 and brine produce frequency-dependent effects, it turns out to be very interesting to analyze the simulated seismic data in the frequency domain. In order to do so, we carry out a spectral decomposition of the data shown in Figures 12c, 13c and 14c. The time-frequency distribution of each seismic trace was computed by inverting the Gabor coefficients of each trace using the procedure outlined by *Sacchi et al.* [2008]. The Gabor coefficients are indexed by two independent variables: time and frequency. We plot the absolute value of the Gabor coefficients of each trace for one frequency at a time. This provides a section with the spatial-temporal distribution of the seismic data at one dominant frequency.

[43] The results are displayed in Figures 15, 16 and 17, where we show, in each case, three plots portraying the absolute value of the Gabor coefficients for $f = 5$, 20 and 50 Hz, respectively. It is interesting to notice that the spatial location of most of the zones with diffuse CO_2 can be clearly appreciated, specially for $f = 5$ and 20 Hz, both for small and big patch sizes, as well as in the homogeneous fluid distribution case. However, the deepest parts of the plume cannot be analyzed so clearly, specially in the case with $a = 0.1$ m, either because of the strong attenuation effects or the complex interference among the various reflectors and their reverberations. Also, the attenuation effects are very evident in the case with a correlation length of 0.1 m. Figures 15 and 17 show no appreciable differences in this regards for $f = 5$ and 20Hz, because in the case $a = 0.01$ m the mesoscopic effects are not very important for these frequencies and hence, their effects in the spectral decomposition are difficult to distinguish. However, for the highest frequency we can observe differences between these two cases, mainly in the lower parts of the plume. These facts are in agreement with Figure 3, since in the smallest patch size case mesoscopic attenuation effects become significant as frequency increases.

[44] Finally, it is also very interesting to notice the relative differences of the intensity of the spectral decomposition when comparing the different frequencies in the case of a correlation length of 0.1 m (Figure 16). This behavior is in agreement with Figures 2 and 3, since in this case compressional phase velocity and quality factor change significantly with frequency and thus, the spectral decomposition shows significant differences as frequency increases. In the case of the smallest patch size, these differences are not so significant, and take place mainly in the lower part of the plume and comparing the data for 20 Hz with those for 50 Hz, in agreement with the Monte Carlo analysis. On the contrary, the changes in the intensity of the spectral decomposition

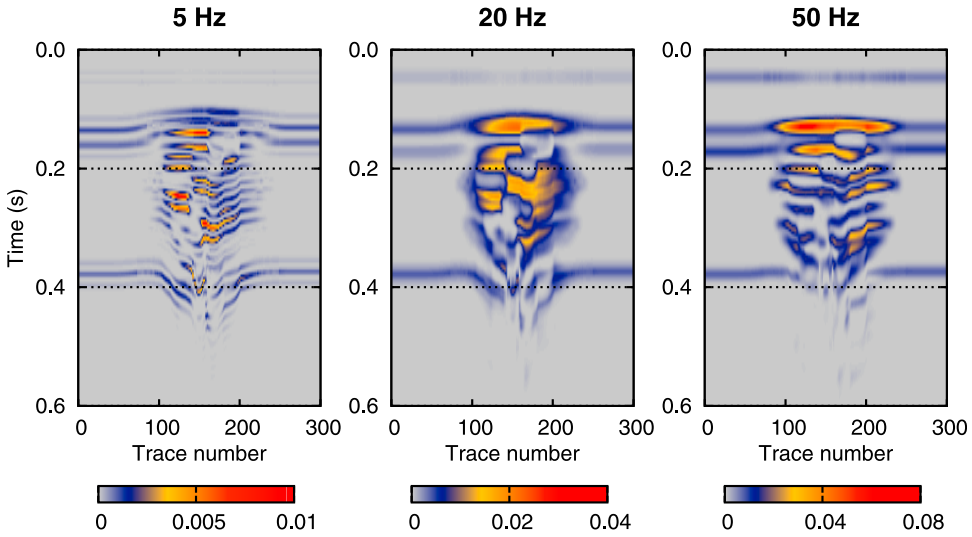

Figure 15. Spectral decomposition of the simulated seismic data corresponding to the patchy model with a correlation length of 0.01 m for three different frequencies: f = 5, 20, and 50 Hz.

when comparing the three plots shown in Figure 17 are negligible, as expected, since in this case frequency-dependent effects are not considered. These results suggest that spectral decomposition may constitute a useful tool to analyze the nature of the fluid distributions, as well as patch size and CO_2 concentrations, which are very important issues in the seismic characterization of seismic monitoring problems.

4. Conclusions

[45] We have analyzed the attenuation and velocity dispersion of compressional seismic waves produced by patchy distributions of CO_2 and brine in poorly consolidated sandstones in the seismic band of frequencies, and their effects on surface seismic data. To this end, we employed a numerical upscaling procedure which permits to determine the wave-induced fluid flow effects of porous rock samples containing mesoscopic-scale heterogeneities.

[46] We first performed a Monte Carlo analysis to determine the statistical behavior of attenuation and velocity dispersion of compressional waves traveling through porous rocks with similar properties as the Utsira Sand, in the Sleipner field, containing quasi-fractal patchy distributions of CO_2 and brine in their pore space. This thorough study let us conclude that these effects are very sensitive to the mean patch size and CO_2 saturation. Particularly, these effects can be remarkably important when the mean patch size is relatively large and the CO_2 saturation is low, specially around 0.1. On the other hand, when patch sizes are very small or CO_2 saturation is very high, these effects can be neglected. In the frame of the Sleipner field, this analysis suggests that wave-induced fluid flow effects may be very significant in the regions containing diffuse CO_2, while they can be neglected in the thin layers containing very high CO_2 concentrations.

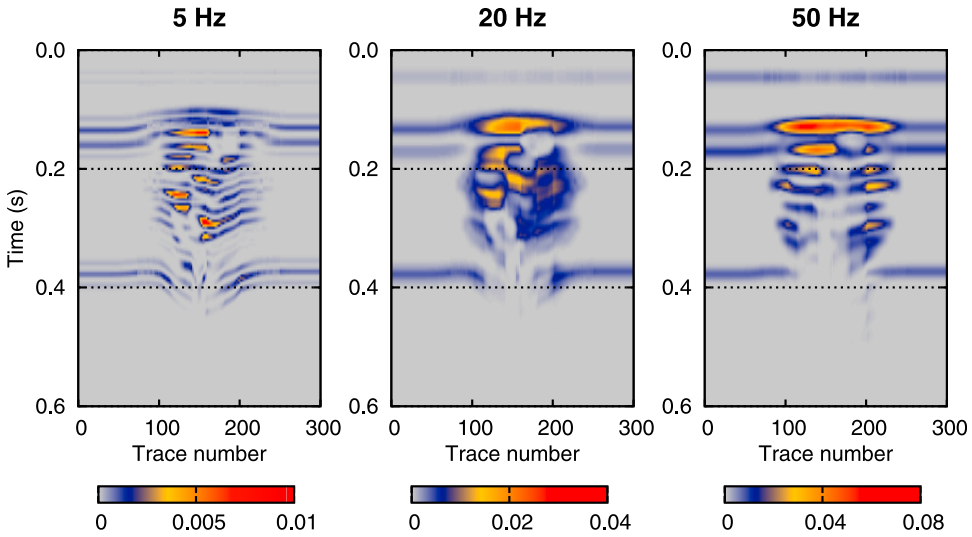

Figure 16. Spectral decomposition of the simulated seismic data corresponding to the patchy model with a correlation length of 0.1 m for three different frequencies: f = 5, 20, and 50 Hz.

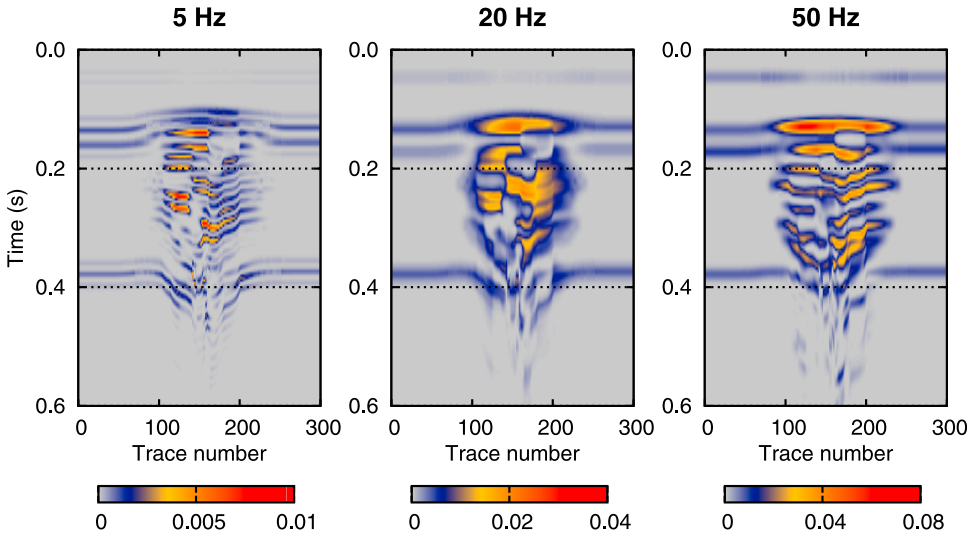

Figure 17. Spectral decomposition of the simulated seismic data corresponding to the homogeneous fluid distribution model for three different frequencies: $f = 5$, 20, and 50 Hz.

[47] In order to analyze wave-induced fluid flow effects on the corresponding surface seismic data, we performed numerical simulations of seismic wave propagation considering reservoir models and CO_2 accumulation patterns having similar characteristics as the CO_2 injection site in the Sleipner field. These numerical experiments showed that conventional surface seismic data may be very sensitive to the nature of the fluid distributions and, in the case of patchy saturation, to the mean size of the heterogeneities. In particular, for a correlation length of 0.01 m the differences between the simulated seismic data considering the patchy distributions and those obtained considering elastic modeling and Gassmann's formula, which assumes a homogeneous distribution of CO_2 and brine, are negligible, as expected since mesoscopic effects are not so important in this case. On the contrary, for relatively large correlations lengths (e.g., 0.1 m) both mesoscopic attenuation and velocity dispersion effects may have a profound impact on surface seismic data, especially in those regions of the plume where the CO_2 is at low concentrations, and thus, the main seismic attributes usually employed in the monitoring of CO_2 injection sites are strongly modified. In terms of the observed velocity pushdown effects, the discrepancy between the pushdown calculated using elastic modeling and Gassmann's formula and that calculated taking into account the patchy nature of the media may be very important. In this sense, relative differences above 20% can be expected, especially when the diffuse CO_2 column thickness is larger than the column thickness of the regions with high CO_2 concentrations, which is the case at the Sleipner field, as described by various authors.

[48] We also carried out a spectral decomposition on the simulated seismic data, which let us observe that this processing technique may be used as an auxiliary tool to delineate spatially the location of the regions containing the diffuse component of CO_2. In addition, analysis of changes in the intensity of the spectral decomposition when comparing different frequencies suggest that this seismic attribute may also help to discriminate the nature of the fluid distributions, a subject that will be investigated in future works.

[49] The results obtained in this work let us conclude that the nature of the fluid distributions, as well as the choice of the modeling technique, constitute very important issues that should not be ignored in the analysis of seismic data whenever more reliable information for the characterization of this kind of reservoirs is required.

Appendix A: Numerical Upscaling Procedure

[50] Figure A1 shows a schematic representation of the undrained oscilatory compressibility test proposed by *Rubino et al.* [2009], where ν is the unit outer normal on the boundaries of the sample and σ is the stress tensor. In this experiment, a representative rock sample containing mesoscopic-scale heterogeneities is subject to a time-harmonic compression of the form $\Delta P e^{j\omega t}$ on its top boundary ($j = \sqrt{-1}$), and no tangential forces are applied on the boundaries of the sample. Also, the solid is neither allowed to move on the bottom boundary nor to have horizontal displacements on the lateral boundaries, and the fluid is not allowed to flow into or out of the sample.

[51] Denoting by V the original volume of the sample, its complex oscillatory volume change $\Delta V(\omega)$ enables us to define the equivalent undrained complex plane wave modulus $\overline{M}_c(\omega)$, by using the relation

$$\frac{\Delta V(\omega)}{V} = -\frac{\Delta P}{\overline{M}_c(\omega)}. \tag{A1}$$

The complex plane wave modulus permits to compute the corresponding complex compressional velocity, given by

$$V_{pc} = \sqrt{\frac{\overline{M}_c(\omega)}{\overline{\rho}_b}}, \tag{A2}$$

where $\overline{\rho}_b$ is the average bulk density of the rock sample. The following relations allow us to estimate the equivalent

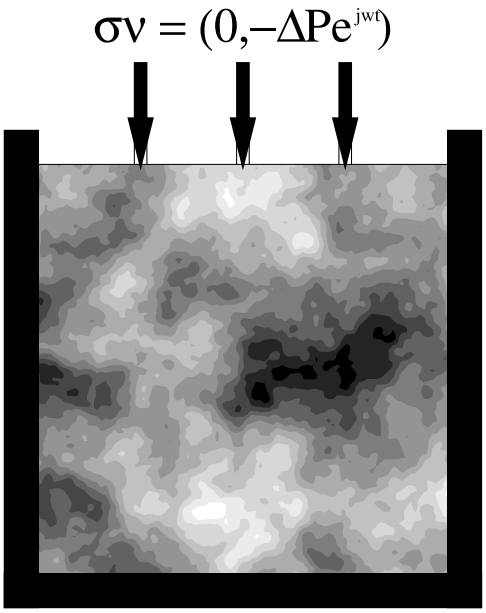

Figure A1. Schematic illustration of an oscillatory compressibility test applied to a representative rock sample.

compressional phase velocity V_p (ω) and quality factor $Q_p(\omega)$ in the form

$$V_p(\omega) = \left[Re\left(\frac{1}{V_{pc}}\right)\right]^{-1}, \qquad \frac{1}{Q_p(\omega)} = \frac{Im\left(V_{pc}^2\right)}{Re\left(V_{pc}^2\right)}. \tag{A3}$$

[52] In order to estimate the complex volume change, *Rubino et al.* [2009] considered a finite element procedure to approximate the solution of Biot's equations of motion [*Biot*, 1956] under the boundary conditions associated with the oscillatory compressibility test. Particularly, they used the bilinear functions to approximate the solid displacement vector, while a closed subspace of the vector part of the Raviart-Thomas-Nedelec space of zero order for the fluid displacement was used. The reader is referred to the work of *Rubino et al.* [2009] for the details of the numerical upscaling procedure.

Appendix B: Modeling

[53] In order to obtain the normal incidence seismic response of a layered viscoelastic medium, let us consider n viscoelastic solid layers embedded between two homogeneous solid viscoelastic halfspaces. Figure B1 shows a simple diagram of the model, and the reflection and transmission rays. For a given frequency ω, each viscoelastic medium is described by its density ρ_i, shear modulus μ_i, compressional phase velocity V_i (ω), and quality factor $Q_i(\omega)$, $0 \le i \le n + 1$.

[54] Then, let a plane harmonic compressional wave of frequency $\omega = 2\pi f$ and unit amplitude propagate in the (x, z) plane arriving at the layered medium with a normal incidence angle. The particle displacements in the top half-space are caused by the contributions of the incident wave and the reflected compressional perturbation, while in the bottom half-space they are produced by the transmitted compressional wave. On the other hand, the displacements within the different beds are obtained by considering two partial wavefields associated with a compressional perturbation traveling upward, and a compressional wave traveling downward within the bed. The displacements in the top half-space, the ith layer, and bottom half-space, can be written respectively as

$$u_i = \begin{cases} e^{j(\omega t - k_0 z)} + R_T(\omega) e^{j(\omega t + k_0 z)} & i = 0, \\ D_i(\omega) e^{j(\omega t - k_i z)} + U_i(\omega) e^{j(\omega t + k_i z)} & 1 \le i \le n, \\ T_T(\omega) e^{j(\omega t - k_{n+1} z)} & i = n + 1. \end{cases} \tag{B1}$$

In this equation, $R_T(\omega)$ and $T_T(\omega)$ are the generalized compressional reflection and transmission coefficients, respectively, while $D_i(\omega)$ and $U_i(\omega)$ are the amplitudes of the contributions associated with the compressional perturbations traveling downward and upward, respectively, within the ith bed. In addition,

$$k_i = \sqrt{\frac{\omega^2 \rho_i}{(\lambda_i + 2\mu_i)}}, \qquad 0 \le i \le n + 1, \tag{B2}$$

are the wave numbers associated with the compressional perturbations in the different media, where λ_i is the Lamé constant of the corresponding medium. Since in this work we analyze heterogeneities associated with pore fluid distributions, we assume that the shear moduli of the different media are frequency independent, real, and equal to the corresponding shear moduli of the dry matrices of the original fluid saturated porous rock.

[55] The next step is to use the elastic properties of each medium to relate the displacement vectors with the stress tensors by means of the Hooke's law. As usual, we require the continuity of the normal displacements and normal stresses through the different interfaces, which leads to a $(2n + 2) \times (2n + 2)$ linear system of equations, where the unknowns are the displacement amplitudes associated with

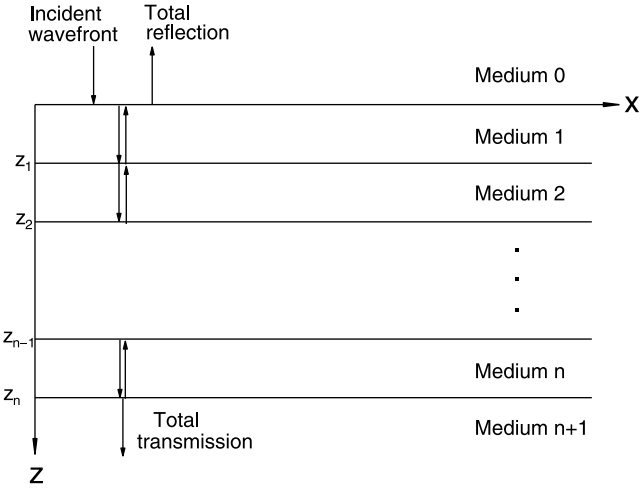

Figure B1. Diagram of the layered model, and the reflection and transmission rays.

the different contributions. The product of the source spectrum and the generalized reflection coefficient $R_T(\omega)$ constitute the Fourier Transform of the seismic data of interest. By applying the inverse Fourier Transform, the seismic trace is obtained.

[56] In order to take into account the viscoelastic nature of the different media composing the model, the wave numbers associated with the compressional waves, k_i, and the Lamé constants, λ_i, should be taken complex and frequency dependent. To compute them, we consider a compressional plane wave propagating through such viscoelastic medium and relate the phase velocity and inverse quality factor with the wave number in the form

$$V_i(\omega) = \frac{\omega}{\mathrm{Re}(k_i)}, \tag{B3}$$

$$\frac{1}{Q_i(\omega)} = -2\frac{\mathrm{Im}(k_i)}{\mathrm{Re}(k_i)}. \tag{B4}$$

Then,

$$k_i = \frac{\omega}{V_i(\omega)}\left[1 - \frac{j}{2Q_i(\omega)}\right]. \tag{B5}$$

In addition, employing equation (B2) we obtain

$$\lambda_i = \rho_i \frac{\omega^2}{k_i^2} - 2\mu_i. \tag{B6}$$

[57] In summary, for each frequency and medium, we apply the oscillatory compressibility test to obtain the equivalent phase velocity and quality factor. Next, using equations (B5) and (B6) we compute k_i and λ_i, which contain the information related to the viscoelastic nature of the medium under consideration.

[58] In order to obtain 2D seismic sections, this procedure is repeated for a large number of locations considering smooth lateral variations of the parameters describing the different models under study. We assume that these data represent a near-offset stack associated with geological models characterized by nearly flat stratigraphy geometry.

[59] **Acknowledgments.** This work was supported in part by a grant from the Swiss National Science Foundation. Partial financial support from CONICET (Argentina) is also acknowledged. We wish to thank Klaus Holliger for his useful comments and suggestions, which helped to improve this work.

References

Arts, R. J., O. Eiken, A. Chadwick, P. Zweigel, L. van der Meer, and G. Kirby (2004a), Seismic monitoring at the Sleipner underground CO_2 storage site (North Sea), in *Geological Storage of CO_2 for Emissions Reduction*, edited by S. J. Baines and R. H. Worden, *Geol. Soc. Spec. Publ.*, *233*, 181–191.

Arts, R. J., O. Eiken, A. Chadwick, P. Zweigel, L. van der Meer, and B. Zinszner (2004b), Monitoring of CO_2 injected at Sleipner using time-lapse seismic data, *Energy*, *29*, 1383–1392.

Arts, R. J., A. Chadwick, O. Eiken, M. Trani, and S. Dortland (2007), Synthetic versus real time-lapse seismic data at the Sleipner CO_2 injection site, paper presented at Society of Exploration Geophysicists International Exposition and 77th Annual Meeting, San Antonio, Tex.

Arts, R. J., A. Chadwick, O. Eiken, S. Thibeau, and S. Nooner (2008), Ten years' experience of monitoring CO_2 injection in the Utsira Sand at Sleipner, offshore Norway, *First Break*, *26*, 65–72.

Biot, M. (1956), Theory of propagation of elastic waves in a fluid-saturated porous solid, *J. Acoust. Soc. Am.*, *28*, 168–171.

Carcione, J., and S. Picotti (2006), P-wave seismic attenuation by slow-wave diffusion: Effects of inhomogeneous rock properties, *Geophysics*, *71*, O1–O8.

Carcione, J., S. Picotti, D. Gei, and G. Rossi (2006), Physics and seismic modeling of monitoring CO_2 storage, *Pure Appl. Geophys.*, *163*, 175–207.

Chadwick, A., R. J. Arts, and O. Eiken (2005), 4D seismic quantification of a growing CO_2 plume at the Sleipner, North Sea, in *Petroleum Geology: North-West Europe and Global Perspectives - Proceedings of the 6th Petroleum Geology Conference*, pp. 1385–1399, Geol. Soc., London.

Chadwick, A., et al. (2010), Quantitative analysis of time-lapse seismic monitoring data at the Sleipner CO_2 storage operation, *Leading Edge*, *29*, 170–177.

Chung, H. and D. Lawton (1995), Frequency characteristics of seismic reflections from thin beds, *Can. J. Explor. Geophys.*, *31*, 32–37.

Duan, Z., N. Møller, and J. Weare (1992), An equation of state for the CH_4-CO_2-H_2O system: I. Pure systems from 0 to 1000°C and 0 to 8000 bar, *Geochim. Cosmochim. Acta*, *56*, 2605–2617.

Gadheri, A., and M. Landrø (2009), Estimation of thickness and velocity changes of injected carbon dioxide layers from prestack time-lapse seismic data, *Geophysics*, *74*, O17–O28.

Lumley, D. (2010), 4D seismic monitoring of CO_2 sequestration, *Leading Edge*, *29*, 150–155.

Lumley, D., D. Sherlock, T. Daley, L. Juang, D. Lawton, R. Masters, M. Verliac, and D. White (2010), Highlights of the 2009 SEG Summer Research Workshop on CO_2 Sequestration, *Leading Edge*, *29*, 138–145.

Pride, S. R., J. G. Berryman, and J. M. Harris (2004), Seismic attenuation due to wave-induced flow, *J. Geophys. Res.*, *109*, B01201, doi:10.1029/2003JB002639.

Rubino, J., and D. Velis (2011), Seismic characterization of thin beds containing patchy carbon dioxide-brine distributions: A study based on numerical simulations, *Geophysics*, in press.

Rubino, J., C. Ravazzoli, and J. Santos (2009), Equivalent viscoelastic solids for heterogeneous fluid-saturated porous rocks, *Geophysics*, *74*, N1–N13.

Sacchi, M. D., S. Kaplan, and M. Naghizadeh (2008), FX-Gabor seismic data reconstruction, paper presented at 71st EAGE Conference and Exhibition, Eur. Assoc. of Geosci. and Eng., Amsterdam.

White, J. (1975), Computed seismic speeds and attenuation in rocks with partial gas saturation, *Geophysics*, *40*, 224–232.

White, J., N. Mikhaylova, and F. Lyakhovitskiy (1975), Low-frequency seismic waves in fluid-saturated layered rocks, *Izv. Acad. Sci. USSR Phys. Solid Earth, Engl. Transl.*, *10*, 654–659.

Zweigel, P., R. J. Arts, A. E. Lothe, and E. B. Lindeberg (2004), Reservoir geology of the Utsira Formation at the first industrial-scale underground CO_2 storage site (Sleipner area, North Sea), in *Geological Storage of CO_2 for Emissions Reduction*, edited by S. J. Baines and R. H. Worden, *Geol. Soc. Spec. Publ.*, *233*, 165–180.

J. G. Rubino, Institute of Geophysics, University of Lausanne, Amphipole Building, CH-1015 Lausanne, Switzerland. (german.rubino@unil.ch)

M. D. Sacchi, Department of Physics, University of Alberta, Edmonton, AB T6G 2J1, Canada.

D. R. Velis, CONICET, Facultad de Ciencias Astronómicas y Geofísicas, Universidad Nacional de La Plata, Paseo del Bosque s/n, La Plata B1900FWA, Argentina.